

Model simulations of the tides in the Barents Sea

by

B. Gjevik, E. Nøst and T. Straume

Department of Mathematics, University of Oslo,
P.O.Box 1053 Blindern, Oslo, Norway.

October 1, 1992

Abstract

A large scale numerical model covering the Nordic Seas and the Arctic Ocean with 25 km grid resolution has been applied to study the tides in the Barents Sea. Tidal charts for elevation and phase are presented for the four tidal constituents M_2 , S_2 , N_2 , and K_1 . Computed harmonic constants for elevation and current have been compared with observations from 35 coastal and pelagic tidal stations. The agreement between model and field data is good for most stations with an overall standard deviation of $\pm 2-5$ cm for amplitude, $\pm 18-30$ deg for phase and $\pm 1-4$ cm/s for current speed. Calculated tidal residual currents show anti-cyclonic eddy circulation over the Svalbard Bank and around Bear Island and Hopen. Particle trajectories and streaklines due to the tidal flow over Svalbardbanken have been calculated and the computed streaklines are found to agree well with observed rifts in the ice cover due to stranded icebergs.

1 Introduction

The Barents Sea (figure 1) forms a relatively shallow basin between the deeper Norwegian Sea to the west and the Arctic Ocean to the north and plays an important role for the interaction with the Arctic. The Barents Sea also has rich fish resources and large oil and gas reserves. It is therefore of general interest to deepen our understanding of the dynamics of this ocean basin.

The tides in the Barents Sea are particularly interesting since the major tidal constituents have amphidromic structures within the area and regions both with very strong and weak tidal currents are found. Also the critical latitude where the M_2 frequency is equal to the inertial frequency passes

through the Barents Sea. This has strong implications for the vertical profile of the tidal current as discussed by Nøst (1992). Dissipation of tidal energy is important in the south-eastern part and the pronounced bottom topography in the west with a steep shelf slope towards the Norwegian Sea has a strong effect on the tide in the western regions.

The major diurnal and semi diurnal constituents (M_2 and K_1) were modeled by Gjevik and Straume (1989) as part of a model area which also covered the Norwegian and the Greenland Seas and the Arctic Ocean with a 50 km grid resolution. We shall subsequently refer to this model as the GS-model. The results for the Barents Sea region were found to agree well with available measurements (Gjevik and Straume, 1989, Gjevik, 1990) and the model predicted amphidromes both for M_2 and K_1 southeast of Bear Island and strong tidal currents over the Svalbard Bank between Bear Island and Svalbard. These structures were not resolved well by the global model by Schwiderski (1986) and he gave no information on the tidal currents. A regional model developed recently at The Arctic and Antarctic Research Institute, St. Petersburg for nearly the same region as the GS-model shows amphidromic structures in the Barents Sea in agreement with the GS-model (private communication Dr. A. Y. Proshutinsky). A reference to this model with some consequences for the ice drift was given by Dmitriev et al. (1991).

The GS-model has later been upgraded and simulations with 25 km grid resolution have been made in order to see the effect of grid refinement. In the new set of simulations we have also included the S_2 and the N_2 constituents. Tables and plots of harmonic constants based on these simulations have been published in an atlas of tides for the Norwegian continental shelf (Gjevik et al., 1990). The atlas has become widely used by engineers and oceanographers, and we have been encouraged to publish a summary of these model results together with a validation study with emphasize on the Barents Sea area.

Over the last 5-10 years there has also been an increased activity for measuring ocean tides in the Barents Sea by various Norwegian institutions (Johansen et al., 1988, Kvamme and Diserud Mildal, 1991). Data for tidal elevation and current have been collected at several pelagic stations particularly in the western part. There is therefore much more data available for model validation now than a few years ago.

The model does not take into account the effect of sea ice on the tides which is of minor importance at least in the open and deeper regions of the Barents Sea. The drift of sea ice due to the tidal current can however be calculated from the model. In order to demonstrate this aspect we have calculated particle trajectories and streaklines in the tidal current field over Svalbardbanken. The results are compared with observed ice rifts in the wake of grounded icebergs (Nilsen et al. 1990, Dmitriev et al. 1991). Calculated traces of ice rifts based on the modeled tidal data on the actual day of satellite imaging of rifts are found to be in good agreement with observations.

2 Model Equations and Numerical Method.

The governing equations for the GS-model are formulated in a Cartesian coordinate system on a stereographic map projection as described by Gjevik and Straume (1989). Here we will only recapitulate the main results. We introduce the coordinate axis (x, y) in the horizontal plane with the corresponding components of the horizontal volume flux (U, V) per unit width. Hence the linearized tidal equations can be written;

$$\frac{\partial U}{\partial t} - fV = -mgh \frac{\partial}{\partial x}(\eta - \bar{\eta}) + A_x + B_x \quad (1)$$

$$\frac{\partial V}{\partial t} + fU = -mgh \frac{\partial}{\partial y}(\eta - \bar{\eta}) + A_y + B_y \quad (2)$$

where m is the map factor, g is the acceleration of gravity, h is the mean depth, f is the Coriolis parameter, η is the vertical displacement of the sea surface from its undisturbed position, and $\bar{\eta}$ is the equilibrium tide or the tide generating potential. (A_x, A_y) are the components of the bottom stress, and (B_x, B_y) are the components of the lateral friction which will be defined subsequently.

The continuity equation reads

$$\frac{\partial \eta}{\partial t} = -m^2 \left[\frac{\partial}{\partial x} \left(\frac{U}{m} \right) + \frac{\partial}{\partial y} \left(\frac{V}{m} \right) \right] \quad (3)$$

and the map factor is defined by:

$$m = \frac{1 + \sin \phi_s}{1 + \sin \phi}$$

where ϕ is the latitude and ϕ_s is the reference latitude for the map scaling.

The bottom stress vector is parameterized by

$$A_x = -\frac{kU}{h}$$

$$A_y = -\frac{kV}{h}$$

where k is the bottom friction coefficient. By choosing

$$k = c_D \frac{\sqrt{U^2 + V^2}}{h}$$

where c_D is the drag coefficient, this corresponds to a quadratic bottom friction law. A linear bottom friction law may be modeled by choosing

$$k = c_D u_s$$

where u_s is a typical velocity scale for the tidal current. The lateral friction is modeled by

$$B_x = \nu m^2 \nabla^2 U$$

$$B_y = \nu m^2 \nabla^2 V$$

where ν is the horizontal eddy viscosity which is related to water depth in a similar way as proposed by Schwiderski (1980);

$$\nu = qh$$

where q is a constant which typically is chosen as 25 m s^{-1}

The equations of motion (1-3) have been discretized on a space staggered C-grid (Mesinger and Arakawa, 1976) with an explicit numerical scheme originally proposed by Sielecki (1968). This scheme has been widely used for depth integrated ocean models and a discussion of its dispersion and stability properties for shelf waves and tides are given by Martinsen et al. (1979) and Gjevik and Straume (1989). The stability criteria for the scheme is

$$\Delta t \leq \frac{\Delta s}{\sqrt{2g(mh)_{max}}}$$

where Δs is half the grid size i.e. the distance between neighbor points where elevation and current are evaluated and h_{max} the maximum water depth. Further details are found in the papers referred above.

3 Model Set-up and Simulations.

The total area covered by the model and the orientation of the grid system is shown in Gjevik and Straume (1989). Along the open boundaries towards the North Atlantic boundary input data have been specified. These data have been taken from model simulations with a North-East Atlantic tidal model developed by a group at Proudman Oceanographic Laboratory, Bidston (Dr. R. A. Flather private communication). The results of these model simulations have been verified by comparing with measurements both from coastal and pelagic tidal stations and the model probably provides the most reliable tidal data set available for the North East Atlantic. There exists various possibilities for implementing elevation or current forcing at the open boundaries as discussed by Gjevik and Straume (1989). In the simulations reported here elevation data have been used for boundary input. This corresponds to model version V (Gjevik and Straume, 1989) which was found to lead to the best results along the Norwegian coast and in the Barents Sea.

The simulations are done with a 25 km grid resolution and simultaneously with four constituents M_2 , S_2 , N_2 , and K_1 which are the dominant semi-diurnal and diurnal constituents. This model version is subsequently denoted model CH. The model CH was started from rest and a spin-up time of 240 hours has proved sufficient for reaching a steady state. After steady state has been reached the model was run for about 660 hours to generate time series of surface elevation and currents. Harmonic constants have been obtained with a conventional harmonic analysis of the time series. The most important model parameters are summarized in table 1.

4 Field Data

For model validation we have applied tidal observations from a set of 35 coastal and pelagic tidal stations with 25 records of tidal elevation and current measurements from several depths at 20 mooring stations (table 2 and figure 1). For many of the coastal stations the available harmonic constants for surface elevation are established from long time series and may therefore be regarded as relatively reliable. For the pelagic stations the observation time has typically been of the order on one months and the corresponding harmonic constants may therefore be subject to considerable error. An indication of the accuracy of the measurements is provided for example by the two independent registrations from position 74° N, 31° E (stations B8 and N, table 2). In general the two data sets are in good agreement and also compare well with model predictions, but the estimated M_2 phase from observations at station B8 is clearly inaccurate (table 3). A similar inaccuracy in the observed orientation angle of the current ellipse is noted (table 4). At most stations where current was recorded, the measurements were made at several depths and the corresponding harmonic constants were calculated at each level (Johansen et al. 1988, Kvamme and Diserud Mildal 1991). In order to make a comparison with the depth average current obtained from model simulations we have calculated an arithmetic mean value of the field data from several depth levels. This averaging procedure also has the effect of reducing the influence of eventual baroclinic tides.

The data from the pelagic stations S1-S6 are particularly interesting since the observations were made during the winter season and under ice. Since some of these stations are located close to other stations where observations have been made during the summer season with no ice cover, this data set can be used for an assessment of the effect of ice on the tide (Nøst, 1992).

5 The M_2 Tide.

The M_2 tidal chart (figure 2) shows a main amphidrome in the Barents Sea southeast of Svalbard (Spitsbergen) and minor amphidromic structures near Franz Josef Land and in the Kara Sea east of Novaja Zemlja. The structure of the main amphidrome with high tidal amplitudes along the coasts of Finnmark in northern Norway and Kola in Russia shows that the M_2 tide in the Barents Sea is mainly a co-oscillating tide driven by the influx from the Norwegian and Greenland Seas as demonstrated by calculating energy fluxes through key sections of the area (Gjevik and Straume 1989, Gjevik 1990).

Comparison between observed and modeled harmonic constants for sea level (table 3) shows good agreement for stations with high amplitude i.e. stations located on or near the northern coasts of Norway and Russia. In the central part of the basin, near the amphidromic point, the differences between observed and modeled data are relatively larger. It should also be noted that the model leads to somewhat larger M_2 amplitudes than observed in the area near Bear Island particularly at stations 7,17,18 and 33 (table 2). The reason for this systematic discrepancy is not clear but may be due to local topographic effects over the shallow Svalbardbanken. The very low value of M_2 amplitude recorded at Kvalvågen on Spitsbergen (station no 9) is most likely incorrect. The measured value leads to a ratio between S_2 and M_2 amplitude close to one which is not representative for the area. The model also shows much higher amplitude for M_2 than observed.

The standard deviation between observed and modeled data for all stations is ± 10.0 cm for amplitude and $\pm 18.8^\circ$ for phase (table 11). If Kvalvågen is excluded the standard deviation becomes ± 5.4 cm for the amplitude.

The observed and modeled parameters of the current ellipse (table 4) are in very good agreement for most stations and the standard deviation for estimates of the major axis is ± 3.6 cm/s for all stations. For a few stations the differences between observed and modeled values are quite large and this contributes significantly to the relatively large value of the standard deviation. The large differences may in some cases be due to measurement errors. In one case where we have independent measurements from the same position (stations B8 and N) it indicates that the measured orientation of the current axis at B8 is inaccurate.

The map in figure 3 shows that the rotation of the current vector is clockwise in the central part of the Barents Sea. There are smaller regions with counter-clockwise rotation in the area around Svalbard and between Novaja Zemlja and Kola. No current measurements were available to verify this prediction.

6 The S_2 Tide.

The amplitude of the S_2 tide in the Barents Sea is from one quarter to one half of the M_2 amplitude. The S_2 tidal chart, figure 4, shows a main amphidromic system with center located southeast of Svalbard and with a similar structure as for M_2 .

Comparison between observed and modeled harmonic constants for sea level (table 5) shows good agreement for most stations and the standard deviation for all stations is ± 2.5 cm for amplitude and $\pm 19.5^\circ$ for phase (table 11).

The observed and modeled parameters for current ellipse (table 6) are also in good agreement for most stations and the standard deviation for estimates of the major axis for all stations is ± 1.1 cm/s (table 11).

The variations in direction of rotation for the current vector shows an almost similar pattern as for M_2 .

7 The N_2 Tide.

The amplitude of the N_2 tide in the Barents Sea varies from one fifth to one quarter of the M_2 amplitude and the location and the structure of the main amphidromic system (figure 5) is nearly the same as for the dominant semi-diurnal constituents M_2 and S_2 .

Comparison between observed and modeled harmonic constants for sea level (table 7) shows good agreement for most station and the standard deviation for all stations is ± 2.5 cm for amplitude and $\pm 21.7^\circ$ for phase (table 11).

The observed and modeled parameters for current ellipse (table 8) are also in good agreement for most stations and the standard deviation for estimates of the major axis for all stations is ± 0.7 cm/s (table 11).

The variations in direction of rotation for the current vector shows an almost similar pattern as for M_2 .

8 The K_1 Tide.

The dominant diurnal constituent K_1 is more affected by the shelf topography than the semi-diurnal constituents. This is particularly noticeable along the shelf edge between Norway and Svalbard and in the Svalbardbanken area near Bear Island (figure 6). This is clearly a consequence of resonance with shelf wave modes in the near diurnal band. Large diurnal currents are found both by field and model data from Svalbardbanken in agreement with earlier observations reported by Huthnance (1981). For some stations particularly near the southeastern slopes of the bank the diurnal current amplitude

is from one half to one third of the M_2 current amplitude. Comparison between observed and modeled harmonic constants for sea level (table 9) shows fair agreement for most stations and the standard deviation for all stations is ± 3.0 cm for amplitude and $\pm 66.8^\circ$ for phase (table 11). The large discrepancies in phases for three stations, B1, Pukhovoy Bay and Vaida Bay, contribute significantly to the large standard deviation for phases. If these three stations are excluded the standard deviation becomes ± 32.0 deg.

The observed and modeled parameters for current ellipse (table 10) are also in good agreement for most stations and the standard deviation for estimates of the major axis for all stations is ± 1.0 cm/s (table 11).

The variations in direction of rotation for the current vector for K_1 shows a similar pattern as for M_2 with the exception for a narrow band of counter clockwise rotation south east of Svalbardbanken. The existence of a zone with counter clockwise rotation of the current vector in this area is also supported by observations although there is not complete agreement on the exact location of the division line between the zones with clockwise and counter clockwise rotation (table 10).

9 Tide Induced Residual Currents

Tidal rectification is important particular in the Svalbardbank area. A systematic model study of the tide induced residual current, with a discussion of the effects of grid resolution and different numerical schemes has recently been performed by Straume (1992).

Figure 7 (from Straume,1992) shows the depth averaged residual current in the Svalbardbanken area obtained by a combined M_2 , S_2 , N_2 and K_1 simulation with a fully non-linear depth averaged model on a 25 km grid. In this simulation an ADI type numerical scheme was applied and nearly the same flow pattern appears with other numerical schemes.

The tide induced residual currents appear to be strongly topographically steered and with current speed up to 1.7 cm/s. A anti-cyclonic eddy is found over the central part of Svalbardbanken between Bear Island and Hopen. This confirms with the results of model simulations by Harms (1991), who simulated the interaction between the M_2 tide and the North Atlantic Current and found strong tidal rectification in this area. Figure 7 also shows weaker eddies around Bear Island and Hopen. Anticyclonic circulation around Bear Island was also found in laboratory models and also seen from field observations (McClimans and Nilsen, 1992). According to McClimans and Nilsen current takes 5-8 days to circle the 20 km diameter island, which requires a current speed of at least 20-30 cm/s.

Particle tracking in the simulated tidal current field near Bear Island leads to transport velocity which are an order less than found by McClimans and Nilsen. Although our grid resolution is poor in the area, this indicates that

that the strong current circulation quoted by these authors is not caused by barotropic tidal effects alone.

Simulations with only the M_2 constituent show nearly the same picture for the residual current as in figure 7, and with maximum velocity up to 1.3 cm/s.

10 Particle trajectories and streaklines in the tidal flow

In the shallow waters of Svalbardbanken between the Bear Island and Hopen, (figure 8) satellite images show curved rifts in the sea ice in the wake of grounded icebergs. Under special conditions the rifts may be preserved for several hours.

The satellite image from 1 June 1988 11 GMT shown by Nilsen et al. (1990) and Dmitriev et al. (1991), reveals a large number of wake rifts. Nilsen et al. (1990) suggested that the curvature of the rifts was determined by the tidal current oscillations superimposed on a southwesterly flowing current. They compared a Lagrangian particle displacement with an 'inverted' rift from the satellite image, but they made no quantitative calculation of the rift forms. Dmitriev et al. (1991) presented computed ice trajectories which were compared with observed rift forms (inverted), but did not map rift forms in time. For this reason we find it interesting to calculate the rift forms by using our model results of the tidal currents in this region.

Firstly, we shall point out the difference between the trajectory of a single particle and the streakline as formed by a sequence of particles released subsequently from a fixed point.

The trajectory is the position of a particle as a function of time. In horizontal Cartesian coordinate system the position of a particle P (x_p, y_p) is defined by

$$\frac{dx_p}{dt} = u(x_p, y_p, t), \quad \frac{dy_p}{dt} = v(x_p, y_p, t) \quad (4)$$

where (u, v) is the Eulerian field velocity. Time integration of these equations gives

$$x_p(t) = x_o + \int_{t_o}^t u dt, \quad y_p(t) = y_o + \int_{t_o}^t v dt \quad (5)$$

where (x_o, y_o) denote the initial position at t_o .

On the other hand, a streakline is formed by the path of particles released continuously from a source point at say (x_o, y_o) . Hence the streakline can be defined by the sequence of n particles released at intervals Δt during the time span from $t = t_o$ to $t = t_o + n\Delta t$

$$x_s = \{x_k; k = 1, \dots, n\}, \quad y_s = \{y_k; k = 1, \dots, n\} \quad (6)$$

where (x_k, y_k) the position of particle k at $t = t_o + n\Delta t$ is given by

$$x_k = x_o + \int_{(k-1)\Delta t}^{n\Delta t} u dt, \quad y_k = y_o + \int_{(k-1)\Delta t}^{n\Delta t} v dt \quad (7)$$

where Δt is chosen small enough to obtain a continuous streakline. The rifts formed in the ice cover by grounded icebergs should idealistically correspond to streaklines traced from the position of the iceberg.

To find the streaklines the tidal current field corresponding to the four dominant tidal constituents M_2 , S_2 , N_2 and K_1 was deduced from the tidal atlas by Gjevik et al (1990) on a 26 km \times 21 km grid for the area where the rifts were observed (figure 8). Eqs (4) were integrated numerically with a Runge-Kutta method by interpolating in the gridded current field with a bi-linear interpolation routine. The computer code used for the numerical integration was based on a program implemented and tested by Joø (1992)

Figure 9a shows examples of calculated streaklines and particle trajectories from a point within the actual area. Figure 9b shows four streaklines computed at six hours time intervals during the tidal cycle. As clearly seen, the streakline and the particle trajectory have opposite curvature, and the curvature depends on when it is being generated in the tidal cycle.

A direct comparison between the computed streaklines and the observed rifts are shown in figure 10, where two observed rifts from the two positions P1 and P2 on the satellite picture shown by Nilsen et al. (1990) are compared with the computed streaklines. A prevailing southwesterly flow of Arctic water is known to exist along the eastern slopes of Svalbardbanken (Nilsen et al 1990, Harms 1991, McClimans and Nilsen, 1992). Harms also show that tidal rectification contributes to this current system. We have therefore computed streaklines both for a purely oscillating tidal flow and a tidal flow superimposed on a uniform residual current in the southwesterly direction. The computed streaklines with a residual current of 25 cm/s in SW direction (line 3) are in good agreement with observations showing that observed rifts from grounded icebergs, can be modeled by streaklines. The length of the computed streaklines in figure 10 as compared to the observed rifts indicate that the rift from position P1 has been preserved for approximately 11 hours, while the rift from P2 has had a shorter lifetime.

Figure 11 shows an overview of streaklines and particle trajectories for the area covered by the satellite picture shown by Nilsen et al. (1990). The location of the area is shown in figure 8. The velocity field used in this example is the tidal current field plus a residual current in the southwest direction.

A refinement of the comparison of computed streaklines and the observed rifts will require more information about the residual current. Wind effects are not taken into account and may also contribute to the deviation between

the computed and observed streaklines. During the observation period the direction of wind varied between north and northeast (Nilsen et al. 1990).

11 Concluding remarks.

The comparison between model and field data encompasses 35 stations with 26 records of tidal elevation and 20 records of mean current measurements. The latter are obtained by averaging over independent measurements from several depth levels.

The agreement between measurements and model is good except for a few stations. The relatively largest deviations between model and field data are found for the diurnal constituent K_1 . For the semi-diurnal constituents M_2 , S_2 , and N_2 the relatively largest deviations are found in the area near the amphidromic points located southeast of Bear Island. The model also leads to somewhat larger M_2 amplitudes than observed over Svalbardbanken.

The largest tidal amplitudes are found along the coasts of Finnmark in Norway and Kola in Russia. Strong tidal currents peaking at 0.8-1.0 m/s at spring are found on Svalbardbanken between Bear Island and Spitsbergen. The tide induced, depth mean, residual current in the Svalbardbanken area has been simulated with a fully nonlinear depth averaged model on a 25 km grid with the constituents M_2 , S_2 , N_2 and K_1 . The results show a anti-cyclonic eddy between Bear Island and Hopen and weaker anti-cyclonic eddies around these islands. The residual current speed is of the order 1 cm/s.

Local effects as for example the detailed structure of the tide in the narrow White Sea east of Kola may not be well resolved by the model but we have not had access to field data for a thorough check of the performance of the model in these areas. Recent observations from Bear Island indicate a large variation in tidal amplitude along the coast from the northern to the southern capes of the island. At the tidal stations near the north cape the M_2 amplitude is 34 cm (table 3) while the newer data from the station near the southern cape shows an M_2 amplitude of 26 cm (Note from Norges Sjøkartverk, Stavanger 17 June 1992). The model shows no indications of large gradients in this area and the observed effect is most likely on a subgrid scale. Despite these deficiencies mentioned above the model provides an accurate overall description of the large scale features of the barotropic tide in the Barents Sea.

An independent check on the accuracy of the predicted tidal current in the Svalbardbanken area is provided by the good correspondence found between calculated streaklines in the tidal flow and the observed rifts in the ice cover in the wake behind grounded icebergs.

Acknowledgment

We wish to thank members of the staff of the following institutions for providing field data for this study; Proudman Oceanographic Laboratory, Bidston, Norges Sjøkartverk, Stavanger, Oceanor, Trondheim and Norsk Polarinstittutt, Oslo. The development of the tidal model was supported by STATOIL, Stavanger. Two of the authors (Nøst and Straume) were supported by research fellowship from the Norwegian Research Council for Science and Humanities (NAVF) and the Norwegian Research Council for Science and Technology (NTNF). We are also grateful to Dr. T. A. McClimans for reading and commenting on an early draft of this paper.

References

- DMITRIEV, N. E., PROSHUTINSKY, A. Y., LØYNING, T. B. and VINJE, T., 1991
Tidal ice dynamics in the area of Svalbard and Franz Josef Land.
Polar Research Vol. 9, No. 2, 193-205.
- GJEVIK, B., 1990
Model Simulations of Tides and Shelf Waves along the Shelves of the Norwegian - Greenland - Barents Seas
In Modelling Marine Systems, Vol 1, chapt. 9, 187-219. Ed. A. M. Davies, CRC Press Inc., Boca Raton, Florida.
- GJEVIK, B., NØST, E. and STRAUME, T., 1990
Atlas of Tides on the Shelves of The Norwegian and The Barents Seas.
Department of Mathematics, University of Oslo, Report F&U-ST 90012 to Statoil, Stavanger.
- GJEVIK, B., and STRAUME, T., 1989
Simulations of the M_2 and the K_1 tide in the Nordic Seas and the Arctic Ocean.
Tellus 41A, 73-96
- HARMS I. H., 1992
A numerical study of the barotropic circulation in the Barents and Kara Seas
Continental Shelf Res. Vol 12 No 9 1043-1068
- HUTHNANCE J. M., 1981 Large tidal currents near Bear Island and related tidal energy losses from the North Atlantic
Deep Sea Res. 28A, 51-70.
- JOHANSEN, Ø., MATHISEN, J.P., and STEINBAKKE, P., 1988
Current Measurements under Ice and Ice Drift Experiment in the Barents Sea.
Report OCE88059, Oceanor, Trondheim, Norway
- JOØ, B., 1992
Metoder for drivbaneberegninger
Cand. Scient thesis, Department of Mathematics, University of Oslo.
- KVAMME, O. B., and DISERUD MILDAL, K., 1991
Water level and current observations in the Barents Sea; Final Report.
Rapport GEO 91-1 Norwegian Hydrographic Service, Stavanger, Norway

- MARTINSEN, E. A., GJEVIK, B., and RØED, L. P., 1979
A numerical model for long barotropic waves and storm surges along the western coast of Norway.
J. Phys. Oceanogr. Vol 9, No 6, 1126-1138
- MCCLIMANS, T. A., and NILSEN, J. H., 1992
Laboratory Simulation of the Ocean Currents in the Barents sea.
Dynamics of Atmosphere and Oceans (In press)
- MESINGER, F., and ARAKAWA, A., 1976
Numerical methods used in atmospheric models.
GARP Publ. ser. WMO, 17, 64 pp.
- NØST, E., 1992
On Computing Current Profiles from Vertically Integrated Numerical Models, with application to the Barents Sea
Sub judice J. Geophys. Res.
- NILSEN, J. H., MCCLIMANS, T. A. and LØVÅS, S. M., 1990
Rift drift in floe flow: iceberg wakes in the Arctic Sea ice.
Continental Shelf Research Vol. 10, No. 1, 81-86
- SCHWIDERSKI, E. W., 1986
Tides.
In The Nordic Seas (ed. B. G. Hurdle): New York Springer-Verlag, 191-209.
- SIELECKI, A., 1968
Scheme for storm surge equations
Mon. Wea. Rev. 96, 150-156
- STRAUME, T., 1992
Testing of different numerical schemes for modelling tides and tide induced residual currents.
Dr. Scient Thesis, University of Oslo. (in preparation)

Tables

Table 1: Model parameters.

<i>Parameters</i>	<i>Model CH</i>
Grid size (km)	25
Bottom friction	quadratic
c_D	0.003
$q (ms^{-1})$	25

Table 2: List of tidal stations.

<i>Station</i>	<i>Coordinates</i>	<i>Map Code</i>	<i>Type/Depth</i>
Bear Island	74°29'N, 19°12'E	7	Oceanic island
Berlevåg	70°52'N, 29°06'E	6	Coastal
Cape Flora	79°57'N, 49°59'E	11	Oceanic island
Cape Zhelaniya	76°56'N, 68°58'E	12	Coastal
Hopen	76°30'N, 25°04'E	8	Oceanic island
Kapp Linne	78°03'N, 13°38'E	10	Coastal
Kirkenes	69°43'N, 30°03'E	4	Coastal
Kvalvågen	77°30'N, 18°12'E	9	Coastal
Pukhovoy Bay	72°39'N, 52°42'E	14	Coastal
Sentralbanken	74°32'N, 30°58'E	16	Pelagic (312 m)
St. Phoque Bay	76°00'N, 59°55'E	13	Coastal
Teriberka Bay	69°11'N, 35°08'E	2	Coastal
Vaida Bay	69°55'N, 32°02'E	3	Coastal
Vardø	70°20'N, 31°06'E	5	Coastal
Yokanskie Island	68°04'N, 39°29'E	1	Coastal
B1	74°59'N, 20°04'E	17	Pelagic (44 m)
B2	74°58'N, 25°04'E	18	Pelagic (191 m)
B3	75°00'N, 30°01'E	19	Pelagic (383 m)
B4	73°01'N, 22°21'E	20	Pelagic (433 m)
B5	76°31'N, 22°34'E	21	Pelagic (216 m)
B6/A	76°24'N, 34°49'E	34	Pelagic (294 m)
B6/B	77°24'N, 30°04'E	35	Pelagic (200 m)
B7	73°01'N, 15°01'E	32	Pelagic (554 m)
N (Nordkappbanken)	72°00'N, 31°00'E	15	Pelagic (328 m)
B8 (Nordkappbanken)	72°00'N, 31°00'E	15	Pelagic (326 m)
B9	75°00'N, 34°58'E	22	Pelagic (193 m)
B10	75°00'N, 15°36'E	33	Pelagic (575 m)
S1A	75°40'N, 21°57'E	23	Pelagic (38 m)
S1B	75°00'N, 21°15'E	24	Pelagic (68 m)
S2	74°34'N, 23°26'E	25	Pelagic (87 m)
S3	75°20'N, 25°00'E	26	Pelagic (157 m)
S4	75°02'N, 27°07'E	27	Pelagic (281 m)
S5	74°51'N, 28°43'E	28	Pelagic (366 m)
A	73°50'N, 20°00'E	29	Pelagic (297 m)
B	73°30'N, 21°30'E	30	Pelagic (473 m)
C	72°20'N, 24°20'E	31	Pelagic (260 m)

Table 3: Harmonic constants for sea level (M_2), phases are relative to Greenwich.

<i>Station</i>	<i>Observed</i>		<i>Model CH</i>	
	<i>H(cm)</i>	<i>$\delta(deg)$</i>	<i>H(cm)</i>	<i>$\delta(deg)$</i>
Bear Island	34	013	41	346
Berlevåg	89	082	83	069
Cape Flora	13	179	24	192
Cape Zhelaniya	15	178	13	176
Hopen	25	215	23	261
Kapp Linne	50	359	52	351
Kirkenes	106	108	101	096
Kvalvågen	26	319	67	309
Pukhovoy Bay	32	159	35	163
Sentralbanken	16	092	11	072
St Phoque Bay	15	176	21	202
Teriberka Bay	121	134	113	127
Vaida Bay	99	085	99	098
Vardø	101	101	94	093
Yokanskie Island	177	183	161	165
B1	28	333	37	340
B2	10	005	18	338
B3	11	094	6	059
B4	41	021	44	008
B5	19	273	22	254
B7	54	332	51	347
N	51	094	50	077
B8	50	117	50	077
B9	18	126	13	130
B10	37	335	45	343
A	36	357	41	352

Table 4: Parameters for current ellipse (M_2). A: Major axis, B: minor axis, θ : orientation of major axis in degree True, Rot.: rotation direction for the current vector, + clockwise, - counterclockwise. The observed values for A and B are arithmetic means calculated from observations from different depth levels. The model values for A and B are calculated depth mean values.

<i>Station</i>	<i>Observed</i>				<i>Model CH</i>			
	A (cm/s)	B (cm/s)	θ (deg)	Rot.	A (cm/s)	B (cm/s)	θ (deg)	Rot.
B1	60.7	41.3	108	+	54.4	44.5	103	+
B2	13.4	5.7	084	+	13.3	4.3	087	+
B3	6.5	1.7	089	+	8.0	0.8	082	+
B4	11.6	2.8	081	+	11.3	2.4	087	+
B5	16.3	4.9	083	+	28.8	8.7	087	+
B6/A	6.1	5.1	069	+	7.0	4.0	080	+
B6/B	8.1	4.8	031	+	8.7	2.1	036	+
B7	6.9	4.3	071	+	6.2	2.9	072	+
N	13.2	1.2	116	+	14.6	0.2	117	+
B8	13.9	1.0	057	+	14.6	0.2	117	+
B9	7.5	5.1	116	+	9.4	4.7	101	+
S1A	50.6	37.7	066	+	55.7	43.9	103	+
S1B	28.3	24.3	100	+	33.2	24.6	098	+
S2	25.0	17.7	091	+	24.0	15.4	090	+
S3	15.0	7.1	090	+	16.2	6.9	087	+
S4	7.5	1.6	076	+	10.2	1.6	081	+
S5	6.6	1.4	082	+	8.5	0.6	074	+
A	13.0	5.9	093	+	12.7	6.5	089	+
B	9.5	2.5	086	+	10.4	2.8	086	+
C	14.1	2.6	097	+	15.1	2.7	089	+

Table 5: Harmonic constants for sea level (S_2), phases are relative to Greenwich.

<i>Station</i>	<i>Observed</i>		<i>Model CH</i>	
	<i>H (cm)</i>	<i>δ(deg)</i>	<i>H (cm)</i>	<i>δ(deg)</i>
Bear Island	13	045	15	030
Berlevåg	25	120	24	112
Cape Flora	4	233	7	252
Cape Zhelaniya	7	221	6	222
Hopen	12	286	10	326
Kapp Linne	16	043	18	041
Kirkenes	30	153	29	142
Kvalvågen	20	349	25	009
Pukhovoy Bay	6	247	10	219
Sentralbanken	3	119	3	075
St Phoque Bay	6	209	5	242
Teriberka Bay	34	175	33	175
Vaida Bay	34	158	29	144
Vardø	29	143	27	139
Yokanskie Island	53	233	49	213
B1	13	015	14	025
B2	6	028	8	019
B3	1	063	3	032
B4	16	060	15	047
B5	11	337	9	321
B7	21	027	18	030
N	13	132	14	118
B8	13	158	14	118
B9	4	223	2	186
B10	21	047	17	029
A	11	033	15	034

Table 6: Parameters for current ellipse (S_2). Further explanations as under table 4.

<i>Station</i>	<i>Observed</i>				<i>Model CH</i>			
	A (cm/s)	B (cm/s)	θ (deg)	Rot.	A (cm/s)	B (cm/s)	θ (deg)	Rot.
B1	13.3	7.5	116	+	13.5	10.7	106	+
B2	4.6	1.5	080	+	3.8	1.1	086	+
B3	3.1	0.7	074	+	2.5	0.2	080	+
B4	3.8	0.6	080	+	3.2	0.6	086	+
B5	5.1	1.7	085	+	8.7	2.2	088	+
B6/A	2.7	1.6	063	+	2.4	1.3	077	+
B6/B	3.4	1.8	146	+	2.9	0.6	035	+
B7	2.2	1.5	059	+	1.7	0.9	067	+
N	3.4	0.2	120	+	4.4	0.0	116	+
B8	3.9	0.1	118	+	4.4	0.0	116	+
B9	3.4	1.8	111	+	3.0	1.5	099	+
S1A	12.2	8.9	068	+	15.3	11.4	108	+
S1B	10.3	8.6	102	+	8.6	6.1	100	+
S2	7.1	4.4	087	+	6.8	4.2	093	+
S3	4.8	2.0	088	+	4.7	1.8	086	+
S4	2.7	0.6	073	+	3.1	0.4	080	+
S5	2.2	0.3	088	+	2.6	0.1	080	+
A	2.8	1.0	096	+	3.4	1.6	089	+
B	3.0	0.9	087	+	2.9	0.7	085	+
C	4.3	1.1	096	+	4.4	0.7	089	+

Table 7: Harmonic constants for sea level (N_2), phases are relative to Greenwich.

<i>Station</i>	<i>Observed</i>		<i>Model CH</i>	
	<i>H(cm)</i>	<i>$\delta(deg)$</i>	<i>H(cm)</i>	<i>$\delta(deg)$</i>
Bear Island	7	357	9	335
Berlevåg	19	055	19	055
Cape Flora	4	145	5	170
Cape Zhelaniya	3	181	3	158
Hopen	4	178	4	238
Kapp Linne	8	332	11	338
Kirkenes	23	083	24	081
Kvalvågen	7	271	13	292
Pukhovoy Bay	6	159	7	143
St Phoque Bay	3	161	4	181
Teriberka Bay	26	101	27	110
Vaida Bay	20	085	23	083
Vardø	21	071	22	078
Yokanskie Island	43	133	35	148
B3	2	077	2	057
B4	11	360	10	357
N	12	065	12	063
B8	12	088	12	063
B9	4	099	3	108
A	8	008	9	341

Table 8: Parameters for current ellipse (N_2). Further explanations as under table 4.

<i>Station</i>	<i>Observed</i>				<i>Model CH</i>			
	A (cm/s)	B (cm/s)	θ (deg)	Rot.	A (cm/s)	B (cm/s)	θ (deg)	Rot.
B2	3.0	1.2	089	+	3.1	1.0	086	+
B3	3.2	1.8	108	+	1.8	0.2	083	+
B4	3.0	0.6	076	+	2.6	0.6	088	+
B6/A	1.7	1.3	023	+	1.5	0.9	080	+
B6/B	1.1	0.5	026	+	1.9	0.5	035	+
B7	1.8	1.1	078	+	1.5	0.7	072	+
N	2.9	0.6	121	+	3.3	0.0	116	+
B8	3.5	0.8	119	+	3.3	0.0	116	+
B9	2.1	1.3	142	+	2.1	1.1	103	+
S1A	8.9	6.5	067	+	12.9	10.7	108	+
S1B	7.8	6.8	087	+	7.9	6.5	100	+
S2	5.1	3.6	065	+	5.5	3.7	089	+
S3	3.2	1.7	088	+	3.7	1.6	086	+
S4	1.5	0.4	074	+	2.3	0.4	082	+
S5	1.7	0.5	090	+	1.9	0.0	117	+
A	4.0	2.1	098	+	3.0	1.6	091	+
B	2.3	0.5	079	+	2.4	0.6	088	+
C	2.9	0.8	104	+	3.5	0.6	090	+

Table 9: Harmonic constants for sea level (K_1), phases are relative to Greenwich.

<i>Station</i>	<i>Observed</i>		<i>Model CH</i>	
	<i>H(cm)</i>	<i>$\delta(deg)$</i>	<i>H(cm)</i>	<i>$\delta(deg)$</i>
Bear Island	5	211	6	166
Berlevåg	10	244	12	230
Cape Flora	7	340	9	337
Cape Zhelaniya	2	148	2	229
Hopen	12	346	7	352
Kapp Linne	7	194	8	216
Kirkenes	12	259	14	243
Kvalvågen	7	334	7	003
Pukhovoy Bay	5	170	7	006
Sentralbanken	4	322	3	304
St Phoque Bay	3	069	4	077
Teriberka Bay	14	266	17	256
Vaida Bay	2	020	15	244
Vardø	12	252	14	242
Yokanskie Island	22	260	23	264
B1	1	014	5	146
B2	4	027	3	036
B3	3	239	3	330
B4	3	216	5	200
B5	11	328	7	325
B7	9	198	7	216
N	7	262	8	247
B8	6	279	8	247
B9	3	329	4	315
B10	5	220	8	202
A	8	145	7	166

Table 10: Parameters for current ellipse (K_1). Further explanations as under table 4.

<i>Station</i>	<i>Observed</i>				<i>Model CH</i>			
	A (cm/s)	B (cm/s)	θ (deg)	Rot.	A (cm/s)	B (cm/s)	θ (deg)	Rot.
B1	19.4	15.1	092	+	19.2	17.8	174	+
B2	1.5	0.5	092	-	2.4	0.0	097	+
B4	1.9	0.2	107	-	2.2	0.1	107	+
B5	6.2	0.7	101	-	6.5	4.6	109	+
B6/A	1.0	0.2	022	+	1.0	0.8	042	+
B6/B	1.6	0.2	008	+	1.8	0.0	028	-
B7	3.9	3.3	176	+	2.6	1.5	091	+
N	1.5	0.2	116	-	2.3	0.3	115	-
B8	1.8	0.3	116	-	2.3	0.3	115	-
B9	1.4	0.8	110	+	1.5	0.9	103	+
S1A	26.3	17.0	043	+	23.1	17.1	008	+
S1B	11.4	9.0	060	+	11.0	9.3	116	+
S2	6.8	4.0	053	+	6.7	5.0	045	+
S3	2.4	0.6	072	+	3.2	1.3	091	+
S4	1.5	0.3	065	-	1.8	0.5	079	-
S5	1.8	0.2	060	+	1.6	0.5	069	-
A	7.5	1.0	135	-	4.6	0.9	111	+
B	3.4	0.1	107	-	2.7	0.6	103	-
C	1.9	0.4	108	+	2.4	0.5	100	+

Table 11: Unbiased estimator of the standard deviation for the regression analysis between observation and model data (all stations included)

<i>Tidal Const.</i>	<i>Amplitude H, cm</i>	<i>Phase δ, deg.</i>	<i>Current A, cm/s</i>
M_2	10.0	18.8	3.6
S_2	2.5	19.5	1.1
N_2	2.5	21.7	0.7
K_1	3.0	66.8	1.0

Figure captions

Figure 1: The bathymetry of the Barents Sea with depth contours in meters and the location of the tidal stations listed in table 2.

Figure 2. Modeled M_2 tidal chart. Equidistance 0.1 m for amplitude and 30 deg. for phase.

Figure 3. Rotation direction for M_2 current vector, \div counterclockwise rotation, $+$ clockwise rotation.

Figure 4. Modeled S_2 tidal chart. Equidistance 0.05 m for amplitude and 30 deg. for phase.

Figure 5. Modeled N_2 tidal chart. Equidistance 0.025 m for amplitude and 30 deg. for phase.

Figure 6. Modeled K_1 tidal chart. Equidistance 0.02 m for amplitude and 30 deg. for phase.

Figure 7. Modeled depth averaged residual currents (cm/s) from simulation with M_2 , S_2 , N_2 and K_1 . Bear Island and Hopen shown by (B) and (H) respectively.

Figure 8. The bathymetry in the shallow shelf waters of Svalbardbanken between the Bear Island and Hopen. The satellite image centered at 75.8°N , 23°E shown by Nilsen et al. (1990) covers the marked area .

Figure 9. (a) Streakline (1) and particle trajectory (2) from a point located within the marked area in figure 7. (b) Streaklines computed with a time interval of six hours; (1) starts at 1800 GMT 30 May and ends at 0600 GMT 1 June, (2) starts at 0000 GMT and ends at 1200 GMT 1 June, (3) starts at 0600 GMT and ends at 1800 GMT 1 June and (4) starts at 1200 GMT and ends at 2400 GMT 1 June 1988. The tidal current field due to the M_2 , S_2 , N_2 and the K_1 constituents with no residual current is used for these calculations.

Figure 10. Computed streaklines for different current fields (full drawn lines 1, 2, 3 and 4) and observed rifts from grounded icebergs (dashed line, 5) at the positions P1 ($74^\circ 57' \text{N } 23^\circ 27' \text{E}$) and P2 ($74^\circ 40' \text{N } 22^\circ 33' \text{E}$). The computed streaklines starts at 0000 GMT and ends at 1100 GMT 1 June 1988, and the velocity field used for the streaklines (1–4) are respectively; (1) tidal current, (2) tidal current + 25 cm/s in WSW direction, (3) tidal current + 25 cm/s in SW direction and (4) tidal current + 25 cm/s in SSW direction

Figure 11. Computed streaklines (full drawn line) and particle trajectories (dashed line) in the shallow shelf waters between the Bear Island and Hopen (marked area in figure 8), starting at 2300 GMT 30 May and ending at 1100 GMT 1 June 1988. The tidal current field is due to the the M_2 , S_2 , N_2 and the K_1 constituents with a residual current of 25 cm/s in SW direction.

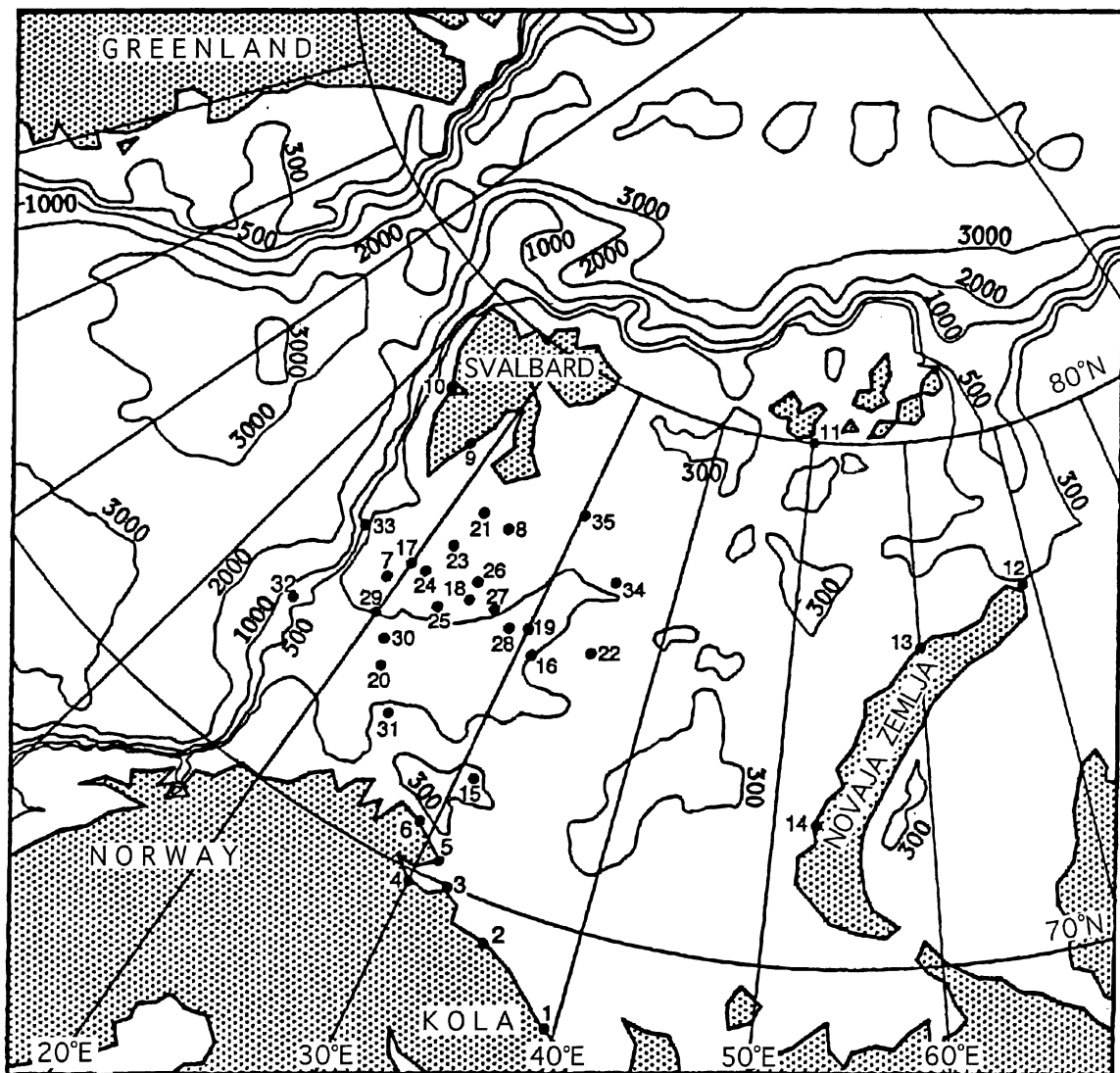


Figure 1:

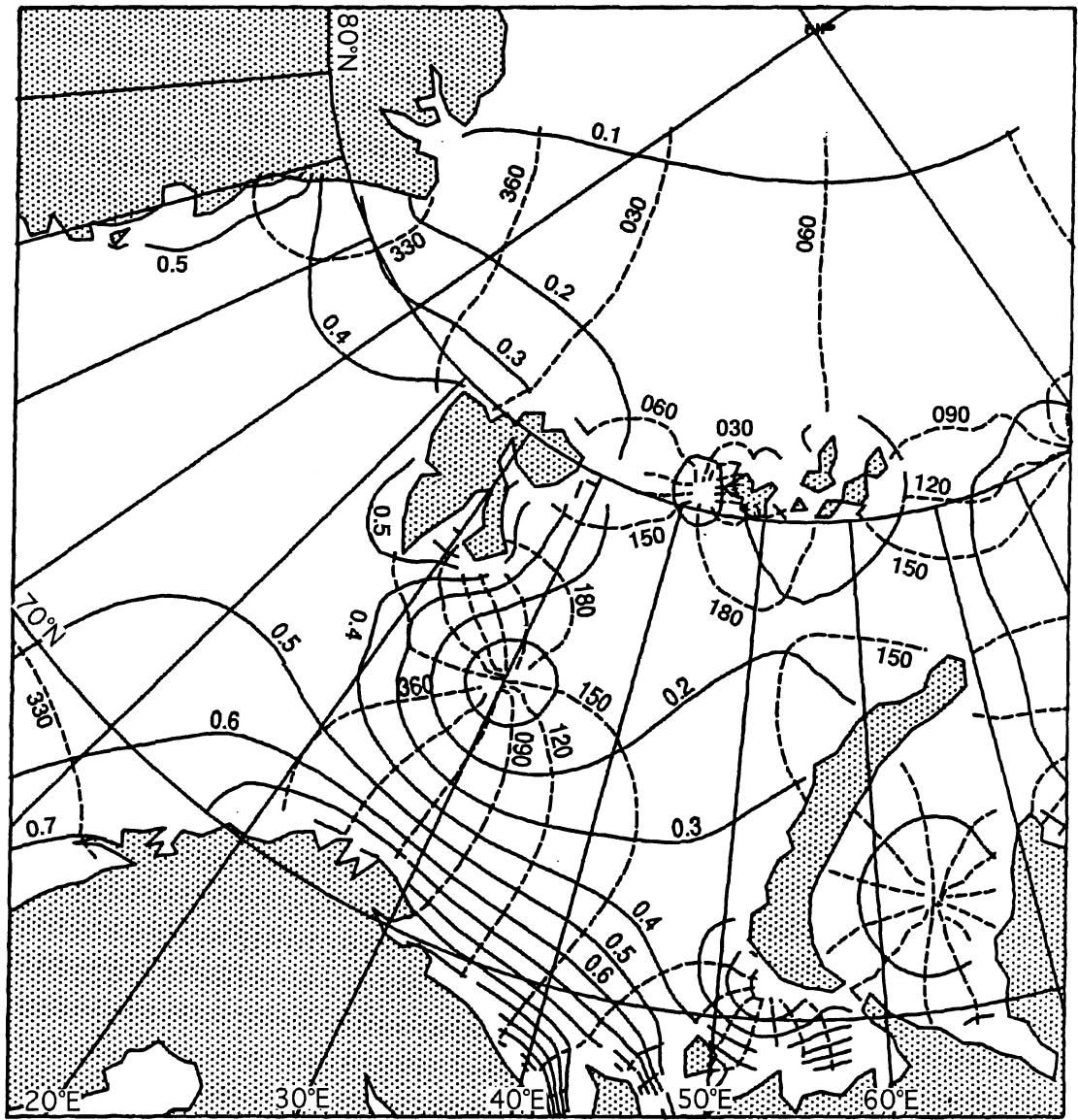


Figure 2:

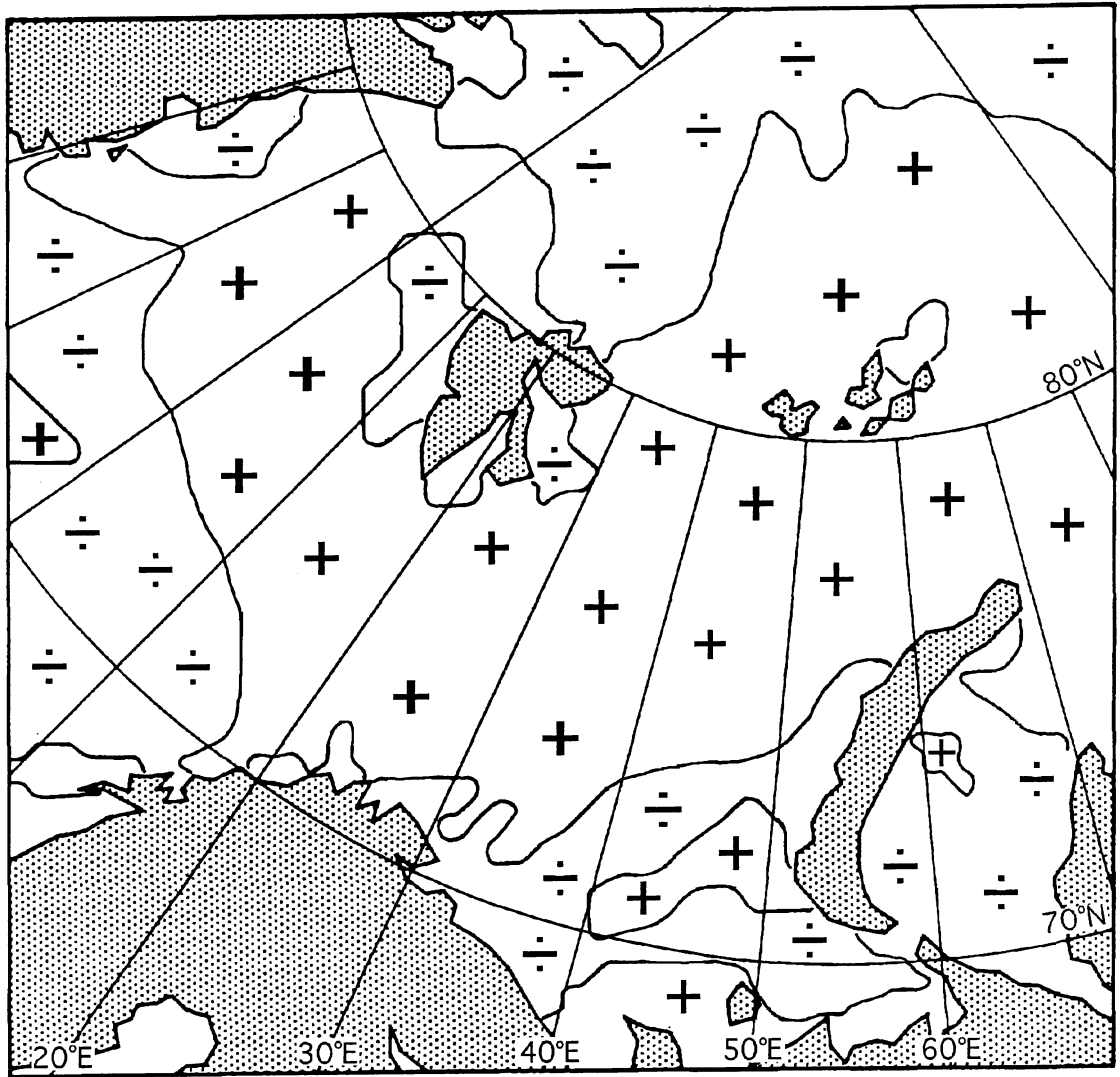


Figure 3:

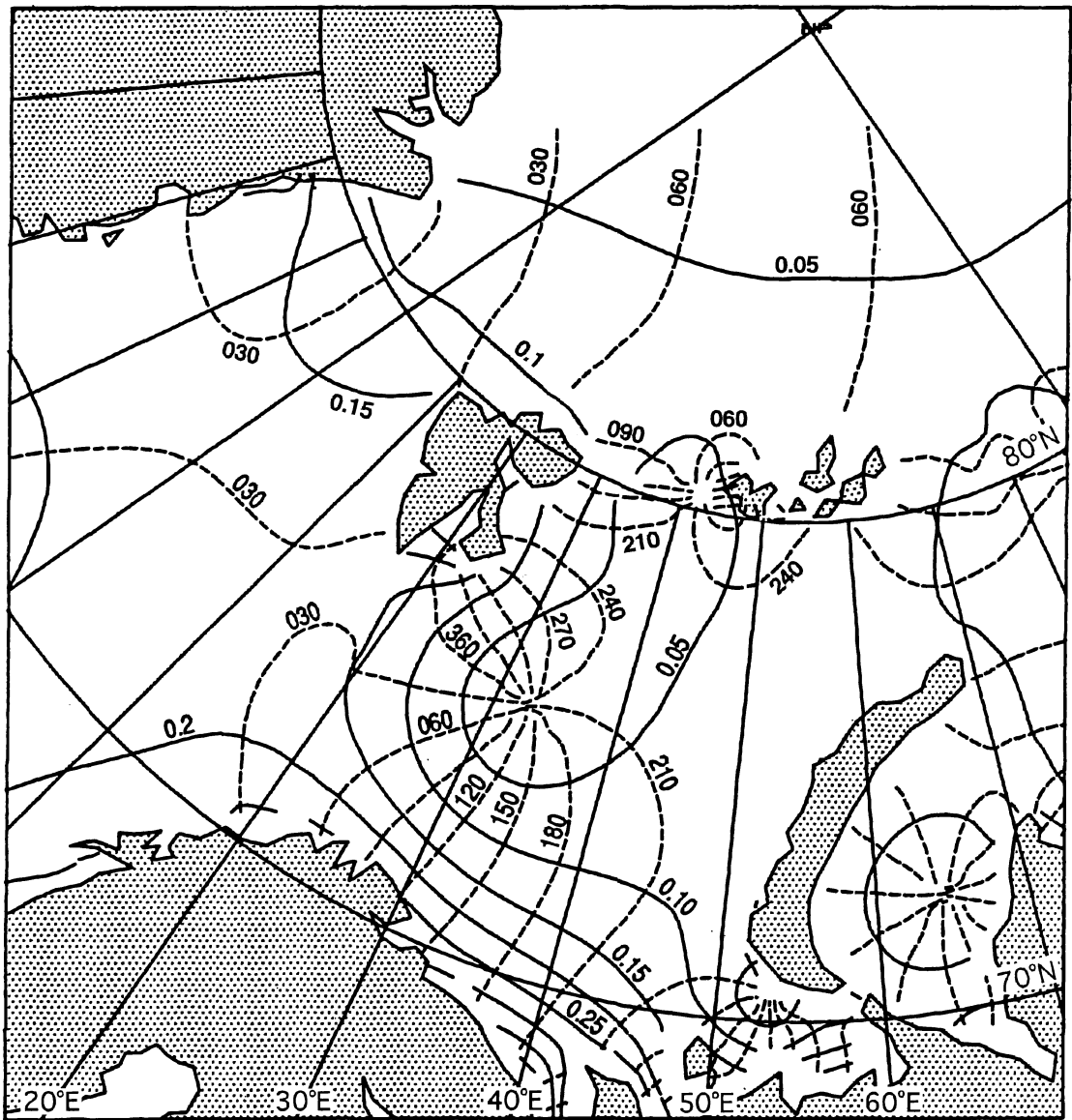


Figure 4:

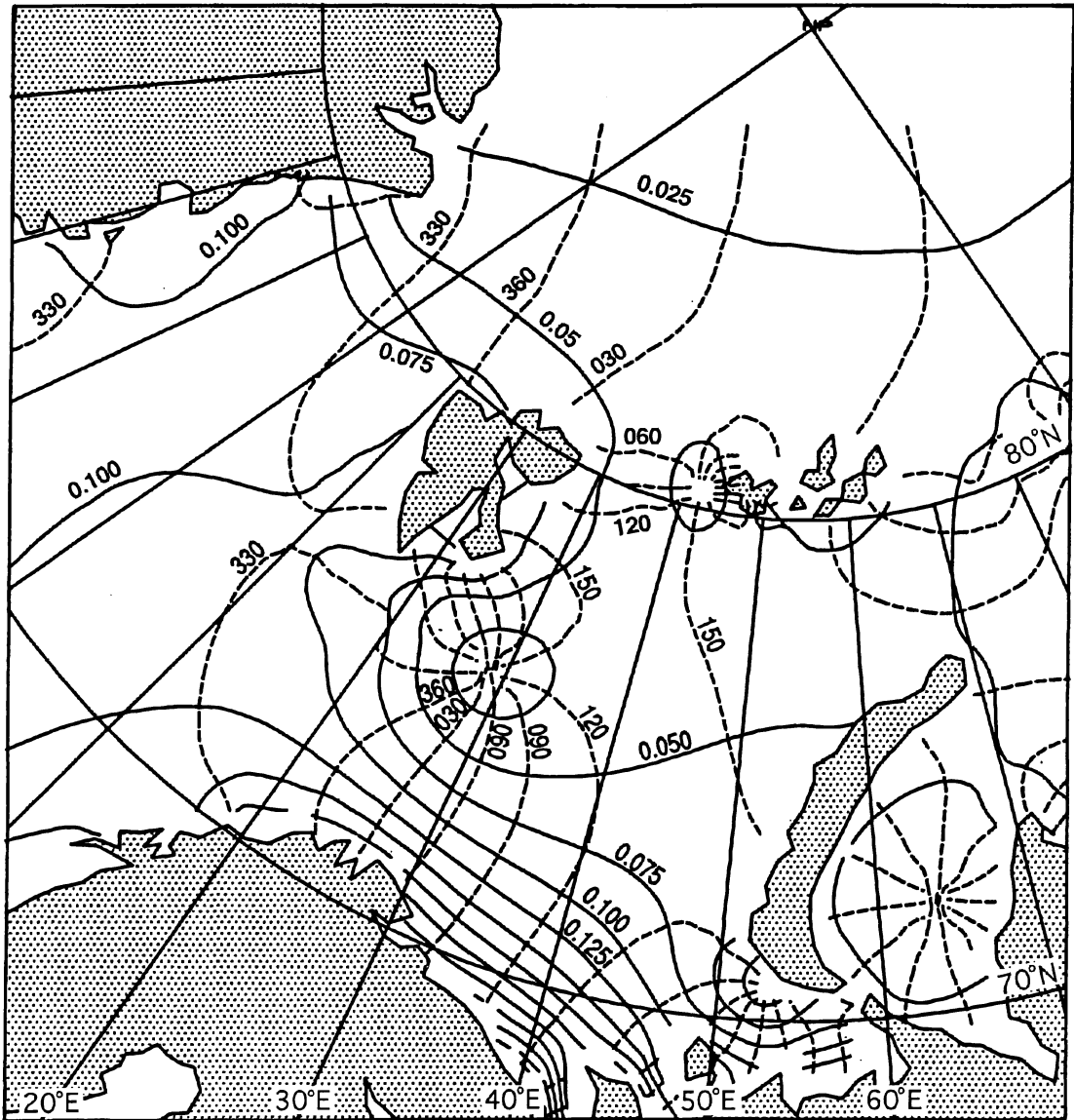


Figure 5:

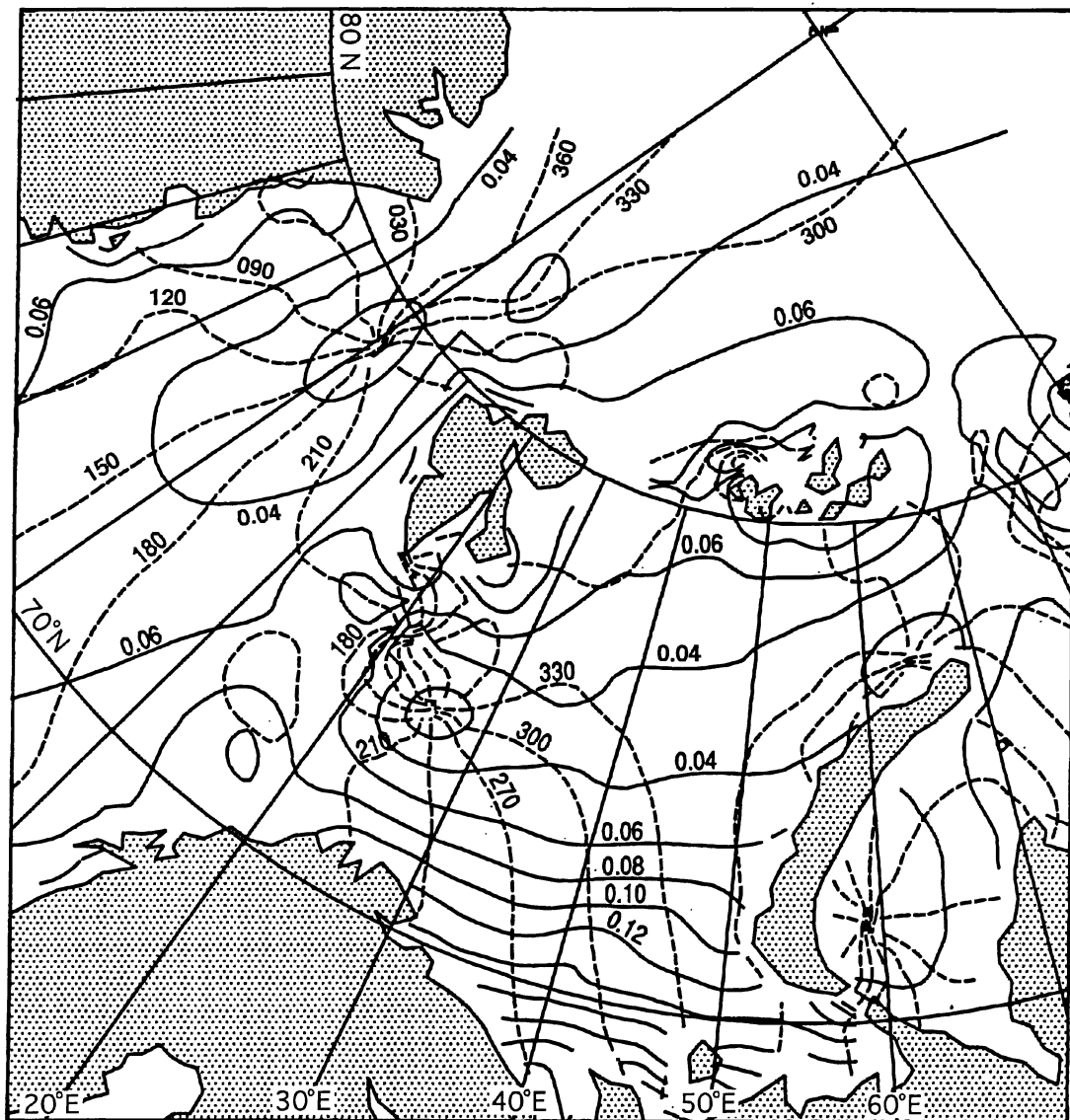
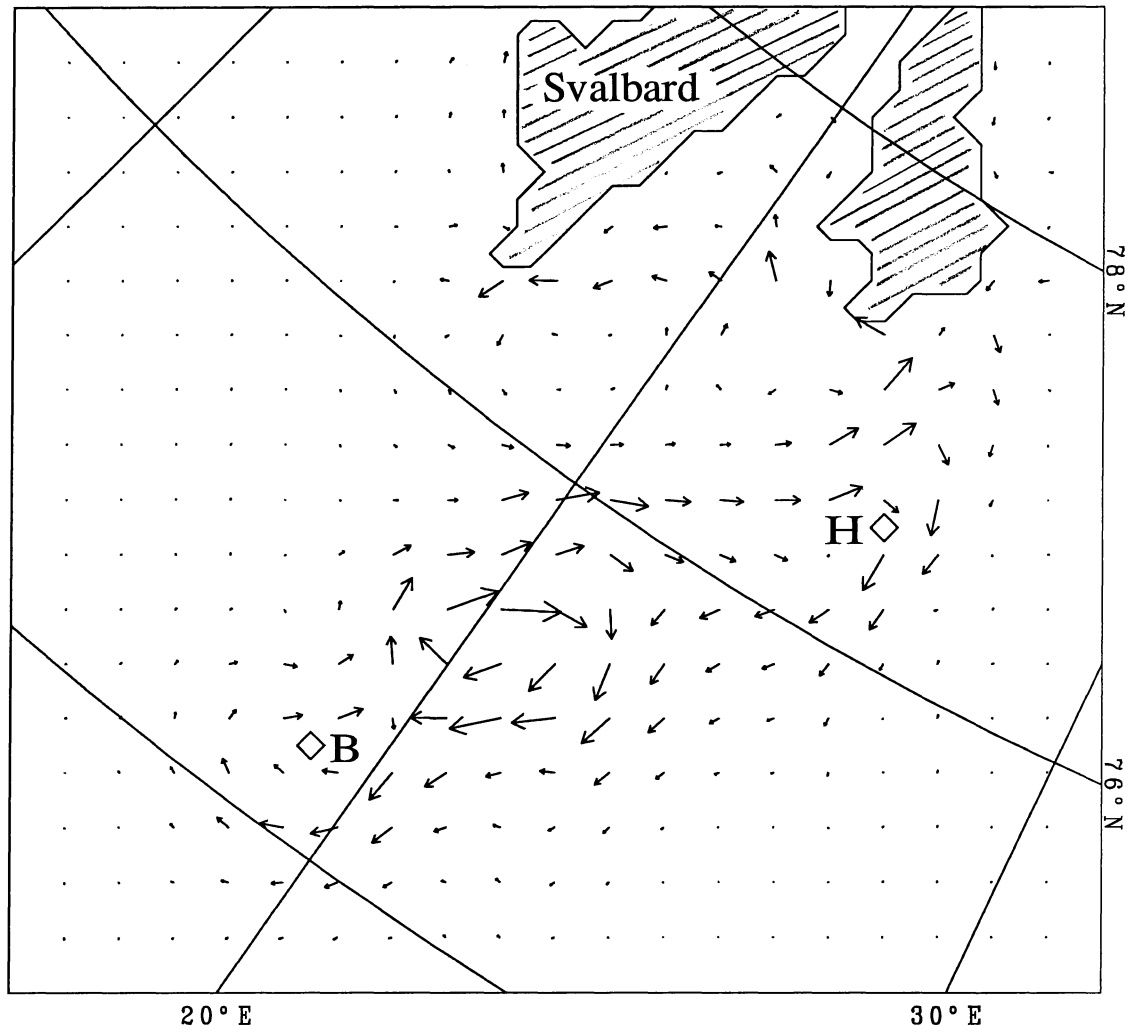


Figure 6:



Linear scaling:
→ 1.5 cm/s

Figure 7:

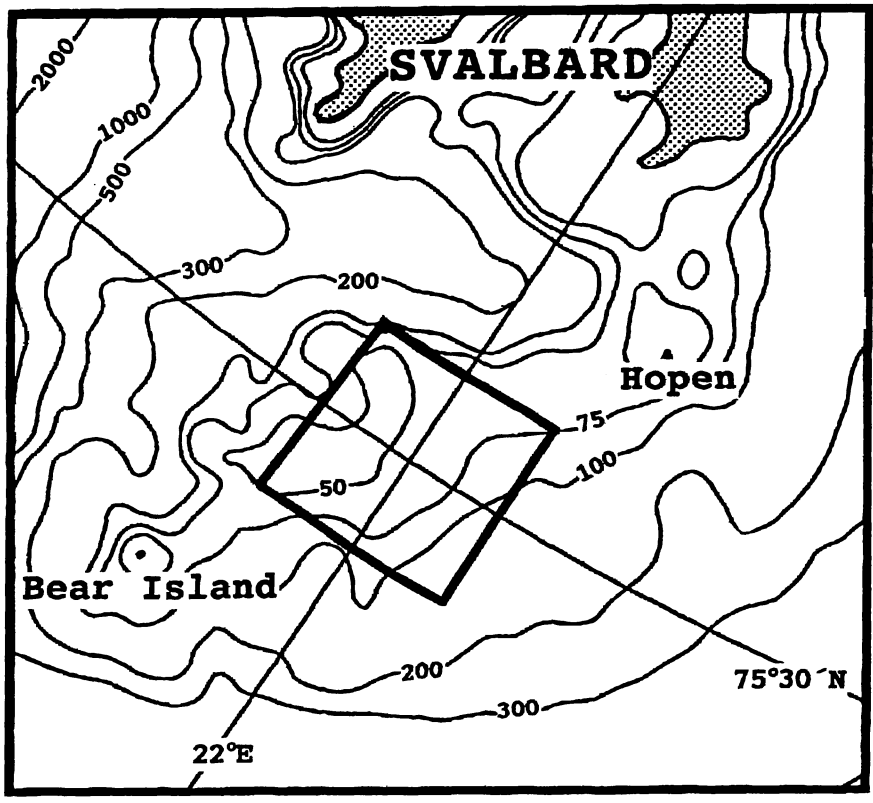


Figure 8:

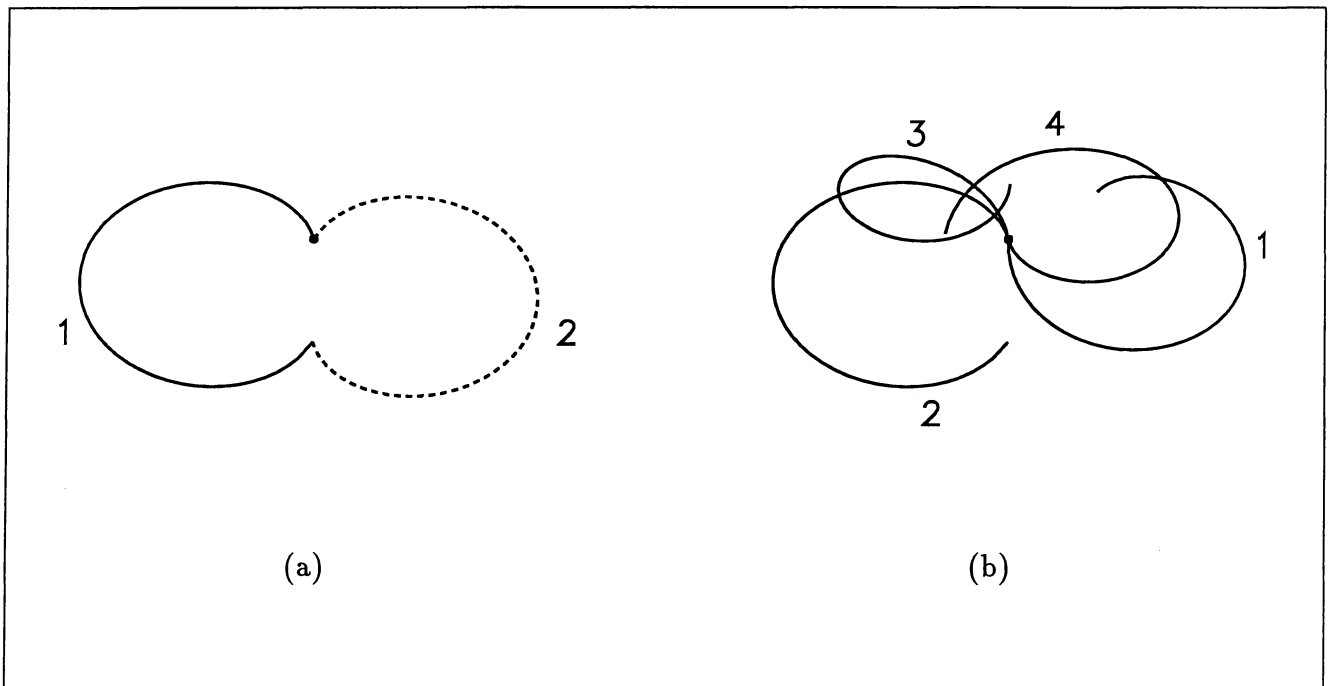


Figure 9:

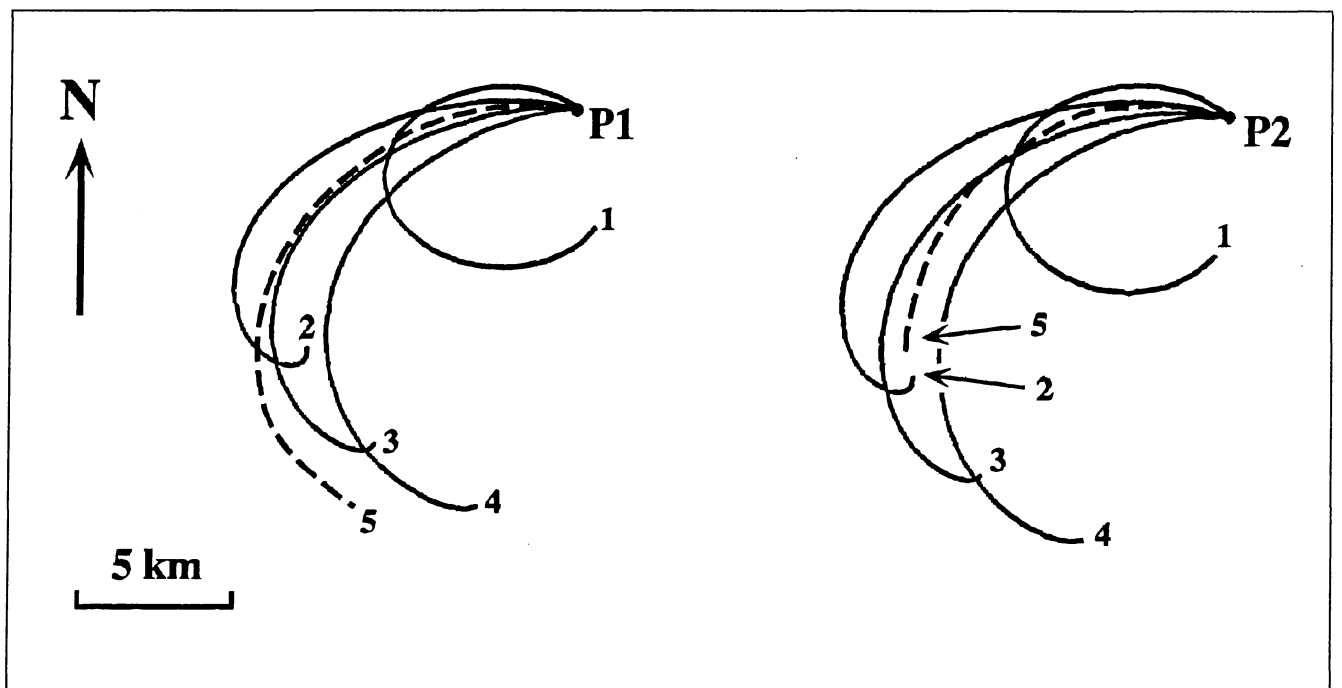


Figure 10:

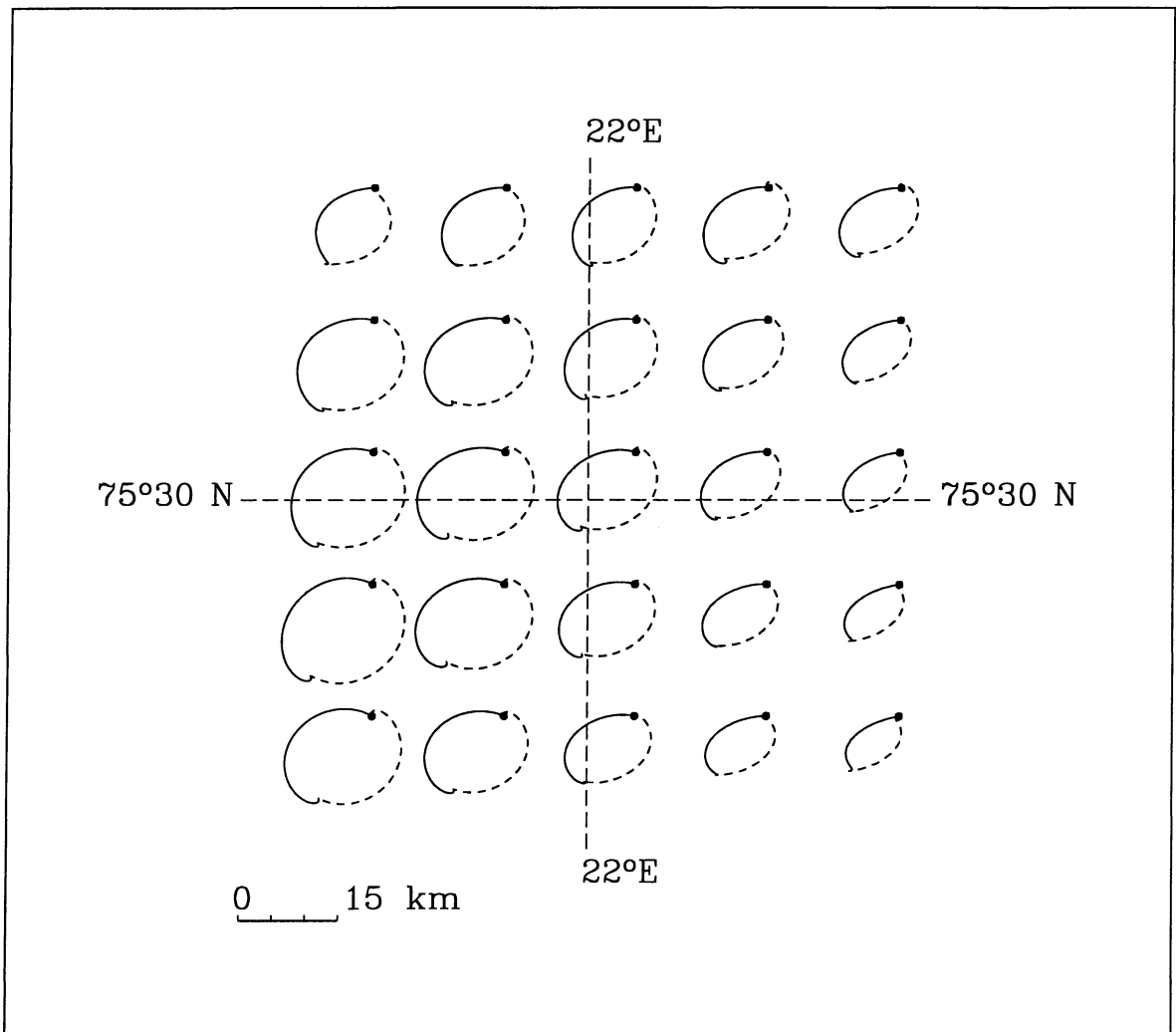


Figure 11: